Title
Potential annual daylighting performance of a high-efficiency daylight redirecting slat system

Journal
Building Simulation, 14(3)

ISSN
1996-3599

Authors
Fernandes, Luís L
Lee, Eleanor S
Thanachareonkit, Anothai
et al.

Publication Date
2021-06-01

DOI
10.1007/s12273-020-0674-6

Peer reviewed

DOI 10.1007/s12273-020-0674-6

BERKELEY LAB

Lawrence Berkeley National Laboratory

Potential annual daylighting performance of a high-efficiency daylight redirecting slat system

Luís L. Fernandes, Eleanor S. Lee, Anothai Thanachareonkit, Stephen E. Selkowitz

Lawrence Berkeley National Laboratory

Energy Technologies Area
August 2020

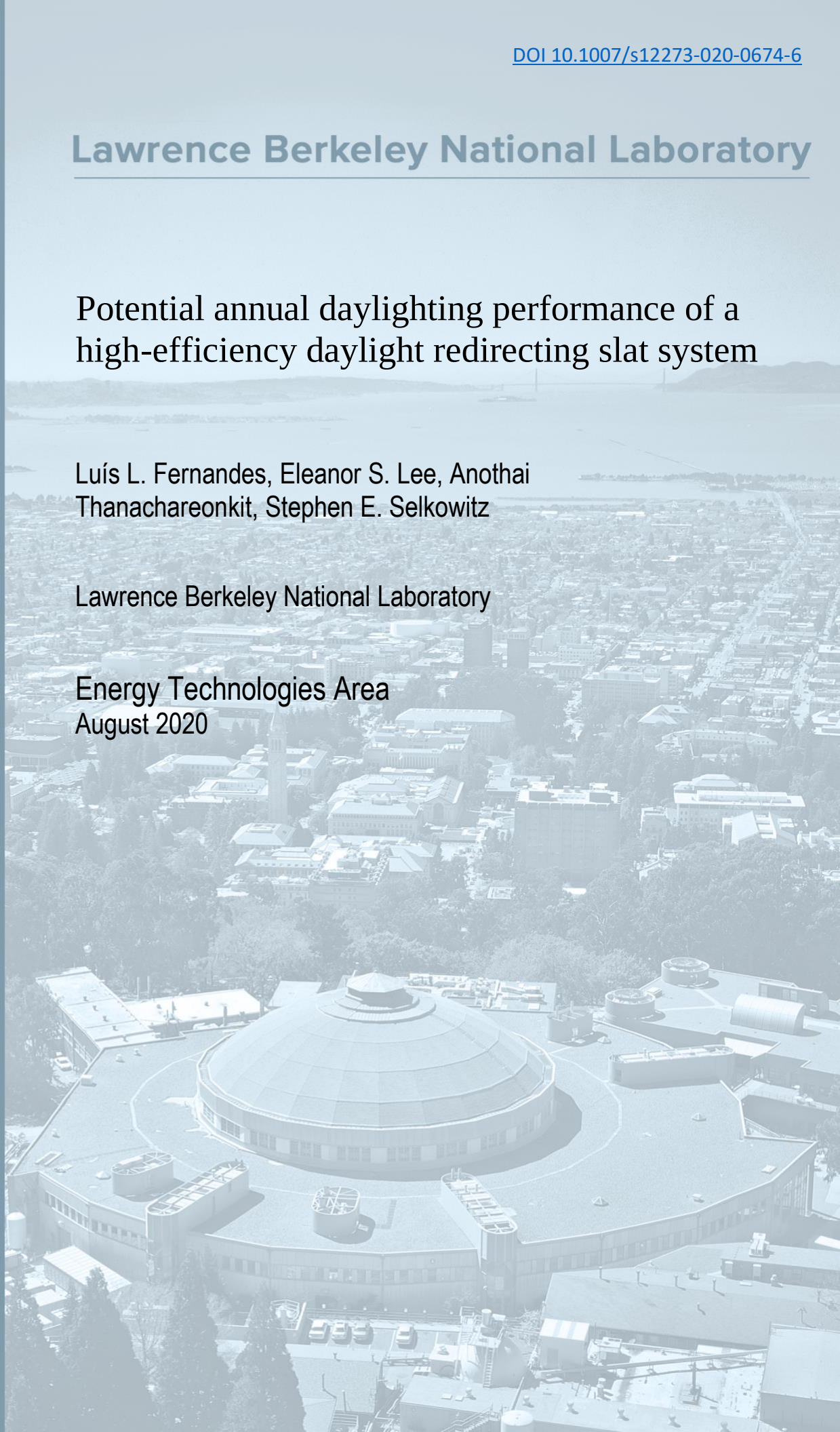

Build Simul
https://doi.org/10.1007/s12273-020-0674-6

Potential annual daylighting performance of a high-efficiency daylight redirecting slat system

Luís L. Fernandes (✉), Eleanor S. Lee, Anothai Thanachareonkit, Stephen E. Selkowitz

Lawrence Berkeley National Laboratory, Berkeley, California, USA

Abstract

While the primary role of window attachments is often to moderate glare and solar heat gains, they are also able to provide additional daylight to interior spaces. For this purpose, a variety of daylight-redirecting window systems have been developed over the past 150 years. Fixed reflective systems (slats/light shelves) or prismatic systems that rely on total internal reflection work well under specific solar conditions, but generally sacrifice performance over a much wider range of incident solar angles and sky conditions. Dynamic systems – typically reflective slats – are more responsive to sun angles but have not been able to achieve optimal performance for glare and daylight redirection efficiency. A previous investigation into an adjustable, reflective blind concept first conceived of in the late 1970s showed promise but was not reduced to practice due to lack of adequate simulation and analysis tools. In this paper, this concept is further developed and its energy and visual comfort performance evaluated for four mid-latitude, temperate climates using ray-tracing simulation techniques. Results indicate significant potential lighting energy savings when compared with conventional automated reflective blinds (2.1–4.9 kWh/(m^2·a), or 14%–42%, depending on climate and orientation) or, especially, manually-operated matte white venetian blinds (1.4–7.9 kWh/(m^2·a), or 9%–54%, depending on climate and orientation), while maintaining acceptable or better visual comfort conditions throughout the interior space.

Keywords

daylighting,
windows,
light-redirecting systems,
dynamic fenestration

Article History

Received: 08 January 2020
Revised: 24 May 2020
Accepted: 08 June 2020

1 Introduction

1.1 Background

In general, window attachments influence the amount of daylight they transmit and the directionality of that transmission. While the primary role of window attachments is often to moderate glare and heat solar gains, they are also able to provide additional daylight to interior spaces. From the perspectives of energy efficiency, indoor environmental quality, and now potentially human health, it is highly desirable to increase the contribution of daylight transmitted through windows to the general illumination of interior spaces. On a bright day, the amount of daylight incident on a square meter of façade is, theoretically, sufficient to light at least 200 m^2 of floor space[1], if one considers no optical losses. Therefore, in theory, sufficient daylight is available; the challenge is to distribute the flux more optimally over the range of solar conditions deeper into the building.

For this purpose, a variety of daylight-redirecting window systems have been developed over the past 150 years. Eacret (1977) provides an overview of patent activity related to beam daylighting systems that goes back to 1885. Before the electric light was well established, a flurry of patent activity at the turn of the 19th century proposed a wide range of refractive and reflective devices to capture and redirect sunlight into buildings (see for example, Pennycuick 1885; Ewen 1897; or Cossmann 1905). Most of this R&D subsided after the advent of more powerful and efficient electric lighting in the 1930s and 1940s, but interest arose again with the advent of the 1973 oil embargo and associated energy crises (Eacret 1977; Baker et al. 1993; Sweitzer 1993). Solutions included conventional reflective and refractive optics and louvers layered in the window system in both fixed and movable designs, light shelf designs that were located on the interior

E-mail: llfernandes@lbl.gov

[1] On a clear sky day, illuminance from the sun on a vertical façade can surpass 70 klx (IES 1984). Assuming no optical losses, this provides enough luminous flux to a square meter of façade to light more than 200 m^2 of floor area at an illuminance of 300 lx.

List of symbols

D	light redirection depth	h_{day}	hour of day
d	vertical distance between slats	L	slat width
d_{max}	maximum vertical distance between slats	$sDA_{X,Y}$	spatial daylight autonomy for reference illuminance X and Y% of the year
d_{min}	minimum vertical distance between slats		
d_{year}	day of year	α	solar incidence angle
E	horizontal illuminance	δ	light redirection angle
h	vertical distance between ceiling and point of solar incidence on slat	ϕ	fraction of full lighting energy power
		θ	slat tilt angle

and exterior of the façade, and active heliostats that reflected sunlight into the building. Size and scale of systems varied, with the more effective solutions integrated with the details of the architectural design. Some systems were static (e.g., most light shelves), while others were manually controlled or automated. A comprehensive review of the broad range of possible daylighting systems at the time was conducted under the International Energy Agency Solar Heating and Cooling Programme Task 21 and is given in Ruck et al. (2001); in addition, Littlefair (1990), Kristensen (1994), Laar and Grimme (2002), Tsangrassoulis (2008, 2016), and Wong (2017) also provide overviews on the variety of daylighting systems.

Solutions occupy different portions of a conceptual solution space whose axes are performance and complexity. The simplest devices are static reflective systems (slats/light shelves) (e.g., Littlefair 1995; Tregenza 1995; Beltran et al. 1996; Konis and Lee 2015) or prismatic systems that rely on total internal reflection (TIR) (e.g., Ruck 1985; Sweitzer 1993; Andersen et al. 2003; Thuot and Andersen 2011; Thanachareonkit et al. 2014; McNeil et al. 2017; Alva et al. 2020). Although they work well under specific solar conditions, many generally sacrifice performance over a much wider range of incident solar angles and sky conditions. Static systems with advanced non-imaging slat profiles have been developed that can redirect useful direct sunlight beyond the perimeter of buildings (up to 4.5 m, or 15 ft, from the windows) while effectively controlling glare (Aizlewood 1993; Heim and Kieszkowski 2006; Konis and Lee 2015; Tsangrassoulis 2016; Moro 2019). This is achieved through slat profiles that reject part or all of the incident sunlight for some solar angles, making it difficult to provide significant illumination to a deep floor plan in a consistent manner. Yip et al. (2015) show significant provision of daylight with a system of this type for an 18 m deep floorplan; however, the floor is illuminated from two sides and the daylighting portion of the window is significantly larger than the view portion of the window (1.9 m high vs. 0.91 m, respectively). Dynamic systems – typically reflective slats – are more responsive to sun angles but have not been able to achieve optimal performance for glare and daylight redirection efficiency, and are more complex and costly, whether mounted on the exterior, interior or between glass. A previous investigation into an adjustable, reflective blind concept first conceived of in the late 1970s (Rosenfeld and Selkowitz 1977) showed promise for admitting daylight deeper into the building with a high degree of glare control but was not reduced to practice due to lack of adequate simulation and analysis tools. Most studies have focused on the perimeter zones of buildings. Ruck et al. (2001) report results from a study with reflective blinds indicating high potential for light redirection but, due to glare, recommend only using reflective blinds above occupant eye height; results are shown only up to 4 m (from the window). Lee et al. (1998) studied a semi-specular automated blind in a 4.57 m deep office, showing significant lighting energy use reduction. Athienitis and Tzempelikos (2002) study the lighting energy savings of a reflective blind covering the whole window and controlled to prevent glare by blocking downward-transmitted direct solar radiation; results are shown only to a distance of 4 m from the window. McGuire (2005) studied an automated reflective blind in which slats were independently controlled in order to combine daylight redirection into the building interior with glare control. The study reports results up to a distance of 10 m, for a blind covering the whole window wall. Although a significant amount of direct sunlight is redirected into the building, some of it is rejected by the slats positioned for glare control. Hashemi (2014) presents a novel automated reflective louver system allowing independent tilt control for every louver slat; results are shown only to a distance of 5.2 m from the window. Blinds with sophisticated slat design (Li et al. 2015) have enhanced capabilities for redirecting daylight while controlling glare and also maintaining a degree of view to the outside. Similarly to other systems, this is achieved at the expense of rejecting some of the incident direct sunlight.

The objective of the study detailed in this paper was to develop the concept first proposed by Rosenfeld and Selkowitz (1977), and assess the technical lighting energy savings potential and impact on other non-energy factors.

The rest of this section describes the fundamental concept of the high-efficiency light redirecting system. Section 2 details the simulation methodology. Section 3 shows the obtained results, including daylight availability provided by the proposed concept; impacts on discomfort glare and daylight quality are also quantified. In Section 4 additional relevant considerations are discussed. A practical implementation of this concept is under development.

1.2 Concept

In accordance with the concept proposed in Rosenfeld and Selkowitz (1977), this study's design objectives and attributes were defined as follows:

- Deep room penetration – provides deep sunlight penetration (up to 12.19 m) without glare; suitable for use in the upper clerestory window of a vertical façade, above eye level, from nominally 2.13 m above the floor to ceiling height;
- Operable – adjusts to different sun angles and sky conditions;
- Optimal control – enables use of all available incident direct beam radiation and minimizes glare under all conditions without requiring secondary shades.

Focusing on the items in the list above, several requirements were defined at the initial stages of development to maximize redirection of useful luminous flux and minimize glare. First, the slats were required to operate over a wide range of solar incident angles, roughly 10°– 70°. When the slats were positioned to their optimal angle to reflect sunlight to the back of the room, two additional requirements were defined: (1) there should be no gaps allowing sunlight to pass downward between the slats into the room, and (2) all sunlight incident on the system should be redirected.

To meet the requirement above, the approach proposed by Rosenfeld and Selkowitz (1977) is to change slat spacing as the solar profile angle changes, with closely spaced slats for low angles and more widely spaced slats for high sun angles (Figure 1). The spacing must change by approximately a factor of three to meet the control requirement.

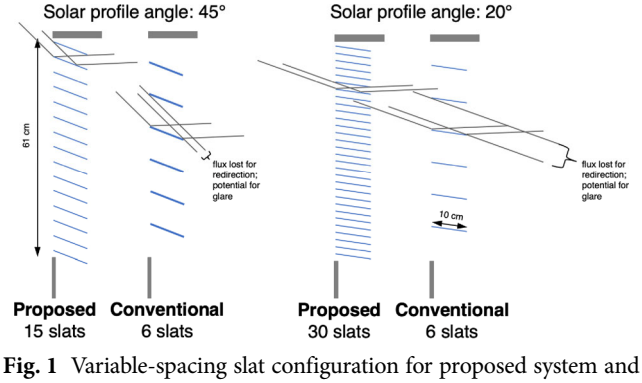

Fig. 1 Variable-spacing slat configuration for proposed system and conventional blind systems used for reference, shown for solar profile angles of 45° and 20°

1.2.1 *Light redirection geometry*

Given a solar profile angle α and a desired redirection depth D, the geometry of redirecting solar flux using a mirrored flat slat is shown in Figure 2, where h is the vertical distance between the ceiling and the point on the slat where the sun's ray reaches the slat. The slat tilt angle θ that will cause solar rays to be redirected to a depth D can then be given by:

$$\theta = \frac{\alpha - \arctan\frac{h}{D}}{2} \tag{1}$$

If one regards the slat shown in Figure 2 as the bottom slat of an array of slats such as the ones shown in Figure 1, incident flux will be redirected towards the ceiling up to a depth of D. There is still the question of determining the optimum spacing of the slats.

There are two extreme cases to be considered for the slat spacing. The upper limit is when slats are spaced so that the uppermost ray passing between two slats is just blocked by the inward-facing edge of the lower slat (Figure 3(a)). If spacing increases beyond this, downward sunlight will be allowed through, which can cause visual discomfort. The relationship between profile angle α, slat angle θ, slat spacing d and slat width L is given by:

$$\tan\alpha = \frac{d + L\sin\theta}{L\cos\theta} \tag{2}$$

The maximum distance d_{max} between slats is then given by solving Eq. (2) for d:

$$d_{max} = L(\tan\alpha\cos\theta - \sin\theta) \tag{3}$$

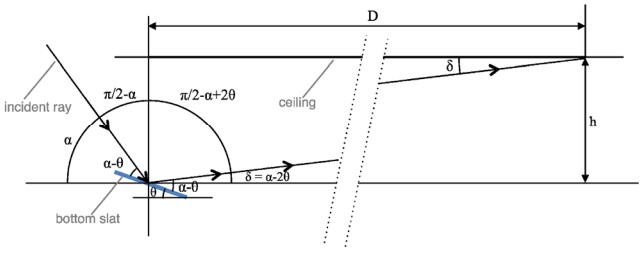

Fig. 2 Geometry of light flux redirection with one flat slat

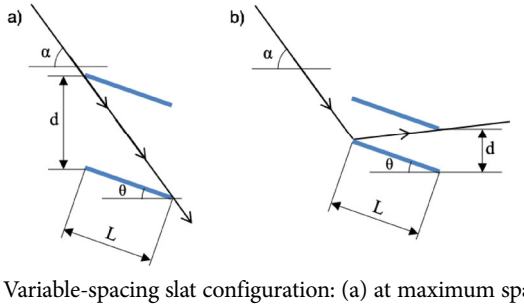

Fig. 3 Variable-spacing slat configuration: (a) at maximum spacing and (b) at minimum spacing

The lower limit for spacing is when slats are spaced so that the reflection of the lowermost ray that hits the lower slat is just let through by the upper slat (Figure 3(b)). In this case, slat spacing is given by:

$$d_{\min} = L\left[\cos\theta\tan\left(\alpha - 2\theta\right) + \sin\theta\right] \quad (4)$$

As long as slat spacing is between these two extremes ($d_{\min}$ and $d_{\max}$), all the flux that reaches the slat system is redirected towards the ceiling. Within this interval, greater spacing will require a smaller number of slats and will lead to a correspondingly smaller number of bright bands on the ceiling. One possible drawback is that the shaded intervals between bright bands will be wider, causing greater illuminance fluctuations at workplane height.

2 Methodology

Daylighting performance of the proposed concept was evaluated using the Radiance lighting simulation software (Ward Larson and Shakespeare 1998), supplemented by its photon-mapping extension (Schregle 2015). Normally, Radiance calculates the trajectory of light *rays* from the point of interest (e.g., a point where illuminance needs to be determined, or a pixel in an image that is to be rendered) back to the light sources in a scene. This process, termed backward ray-tracing, is computationally more efficient than tracing light rays from light sources (termed forward ray-tracing), because not all those rays are relevant to the calculation (they may end up in parts of the scene that are not of interest, i.e., outside an image that needs to be rendered). In certain applications, however, such as modeling the transmission of daylight through windows, it is computationally advantageous to model the transmission of light through the window using forward ray-tracing. This is especially the case if the window contains mirrored surfaces that can produce complex optical effects. Within Radiance, there are two methods to perform forward ray-tracing through windows in order to achieve a more efficient computation. The first method uses a Radiance sub-program called *mkillum*. It can deal with most types of window systems. The second method is an extension of Radiance that uses photon mapping. This method was developed with the goal of more accurately modeling some optical behaviors that *mkillum* could not easily model, such as the reflected patterns on room surfaces caused by curved mirrored slats. In this paper, the photon mapping method was used in order to more accurately model the behavior of the light redirecting system. The matrix methods that can be used with Radiance in order to significantly shorten computation time for annual simulations (Lee et al. 2018) were considered but not used for simulating the behavior of this specific system. This was due to the potentially high number of pre-computed matrices that might be necessary to accurately represent every single slat position/angle combination throughout the year; this would invalidade the significant computational advantage that matrix methods generally provide. The control logic for the annual simulations performed in this study was implemented using *bash* shell scripts running on a Linux-based operating system.

2.1 Space model

The space modeled had a façade 30.5 m wide and was 15.3 m deep (Figure 4). It was aimed at representing a space in an ordinary open-plan office building. The ceiling was 2.74 m above the floor. The façade had a 61 cm high opening starting at 2.13 m above the floor, going all the way to the height of the ceiling. The reflectance of the interior surfaces was 0.8, 0.5 and 0.2 for ceiling, walls and floor, respectively. These surfaces were modeled as perfectly diffuse. In order to maintain computation time within manageable limits, no furniture or other interior objects were modeled. The opening had two glass panes 10.01 cm apart to accommodate the width of the slats, which were 10.00 cm wide and placed between the two glass layers. The outside pane was modeled as 6 mm clear glass. The inside pane was modeled as 6 mm clear glass with a spectrally-selective low-emittance coating on surface 3 (i.e. oriented towards the exterior). The solar-optical properties of each glass layer are shown in Table 1. The geometry of the window is shown in Figure 5. Electric lighting was not modeled.

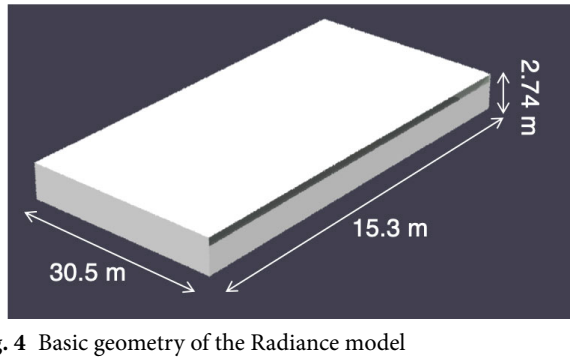

Fig. 4 Basic geometry of the Radiance model

Table 1 Solar optical properties of glass layers in Radiance model

		Outward glass layer	Inward glass layer
Composition		6 mm clear glass	6 mm clear glass with spectrally-selective low-e coating
Visible	Transmittance	0.88	0.72
	Front reflectance	0.08	0.08
	Back reflectance	0.08	0.06

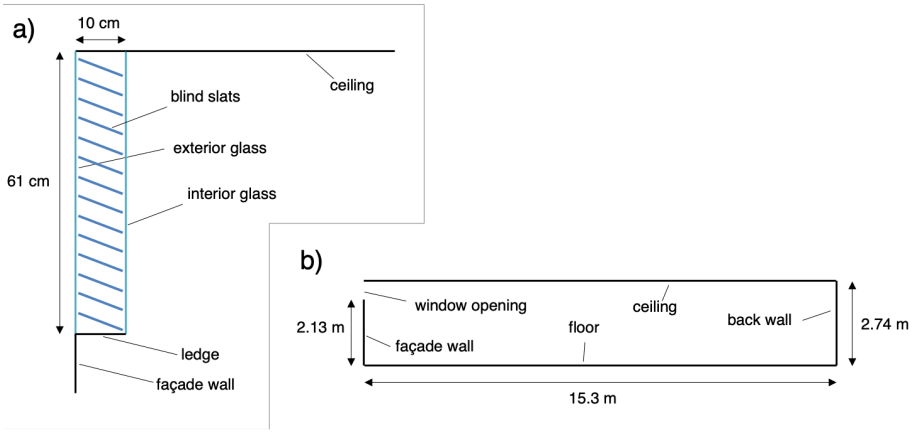

Fig. 5 Simulation geometry: (a) geometry of the modeled window; (b) section view through the modeled space

2.2 Model of the fenestration opening

Five different window configurations were modeled. The first (Configuration A) is the proposed high-efficiency, light-redirecting blind system. Configuration B is based on a commercially-available automated reflective blind system. Configuration C is a matte white manually-operated venetian blind. The mode of operation modeled for each configuration is described below. In order to be able to separate the effects of automation and slat finish, two other configurations were simulated: (1) Configuration Bdiff, with the slats operated like for Configuration B but having a diffuse finish like in Configuration C and (2) Configuration Cmirr, with the slats operated like for Configuration C but having a mirrored finish like in Configuration B. All configurations are summarized in Table 2.

2.2.1 Configuration A: Proposed system

The upward-facing surface of the slats was modeled as having no diffuse reflection and a reflectance of 0.99, a reasonable approximation of high-end commercially available reflective films (see for example 3M (2017))[2]. The downward-facing surface of these slats was modeled as a perfectly diffuse material with 0.7 reflectance, representing a matte white finish. The system was in operation whenever direct sunlight could reach the façade[3]. When the sun was below the horizon

[2] In a practically implemented system, factors such as dust and dirt can reduce surface reflectance. Based on typical dirt depreciation factors for electric luminaires (IES 2000), reflectance could be expected to decrease by 4.1 percentage points after six months (6.7 after a year) for an exposed surface that is not cleaned. These issues can be mitigated or eliminated by, for example, encasing the system in a sealed enclosure such as an insulated glazing unit, or using anti-electrostatic techniques to repel dust from the surface of the slats.

[3] Sun position was calculated using standard formulas – see for example, IES (1984).

Table 2 Blind configurations for annual simulations

Configuration	Description	Slats	Control algorithm
A	Proposed system: automated, variable slat height, reflective blind	Reflective: flat, upward-facing surface specular (r=0.99), downward-facing surface perfectly diffuse (r=0.70)	Automated: Blinds raised when sky overcast, sun below horizon or behind façade plane; Slat height and angle determined using Eqs. (1)–(3), adjusted every hour
B	Conventional automated reflective blind	Reflective: flat, upward-facing surface specular (r=0.99), downward-facing surface perfectly diffuse (r=0.70)	Automated: Blinds raised when sky overcast, sun below horizon or behind façade plane; Slat angle adjusted every hour so that downward transmission of direct sun is always blocked (Eq. (3))
Bdiff	Commercially-available automated reflective blind	Same as C	Same as B
C	Matte white manually-operated blind	Diffuse: flat, upward-facing and downward-facing surfaces perfectly diffuse (r=0.70)	Manually-operated: Blinds start day raised; blinds lowered when DGI* ≥ 24 or DGP* ≥ 0.38, stay lowered rest of day; Slat angle set so that there is no downward transmission of direct sun for rest of day (Eq. (3))
Cmirr	Matte white manually-operated blind	Same as B	Same as C

* DGI and DGP are Daylight Glare Index and Daylight Glare Probability, respectively. For more detail on these metrics, see Sections 2.2.4 and 2.3.2.

or behind the façade, the slats were raised. For each time step, sky cover was determined from the ratio between direct normal and diffuse horizontal irradiance[4]. If that ratio was less than 0.05[5], the sky was considered to be overcast and the slats were retracted. When the sky was not overcast, and if the sun was not below the horizon or behind the façade, slats were lowered with slat spacing and angle determined using Eqs. (1)–(4), for a redirection depth D of 12 m (39.4 ft) and slat width L of 7.72 cm. Slat angle and spacing are shown in Figure 6 for south orientation and 38°N latitude, on the solstices and fall equinox if sunny.

2.2.2 Configuration B: Conventional automated reflective venetian blind

This configuration was modeled using the same slats as for Configuration A in order to isolate variable spacing as a factor in blind performance. Slat spacing was held constant and was 4.59 cm, based on a slat spacing-to-width ratio of 0.59, obtained from the specifications for a commercially-available system. The system was controlled similarly to Configuration A, with the slats only deployed when the sky was not overcast and when the sun was above the horizon and in front of the façade plane. The only difference was that slat angle was determined so that slats were at the most open position that also blocked downward transmission of direct solar radiation. This was done by solving Eq. (2) for θ with d and α known. Beyond performing basic glare control by blocking downward transmission of direct sunlight, this control algorithm privileges the admission of the maximum amount possible of daylight to the detriment of better glare control. This scenario is intended to represent an upper limit for the lighting energy savings achievable by the currently available automated venetian blind systems.

2.2.3 Configuration Bdiff: Same as B but with matte white slats

This configuration was modeled similarly to Configuration B, with the exception that the slat finish was perfectly diffuse with 0.7 reflectance on both upward- and downward-facing surfaces. The intent of simulating this configuration was to be able to separate the effects of the control algorithm from those of the slat finish.

2.2.4 Configuration C: Manually-operated matte white venetian blind

For similar reasons to those stated above for Configuration B, this configuration was modeled with slats similar to the ones used for Configurations A and B. The only difference is that the upward-facing surface was perfectly diffuse with 0.7 reflectance – the same as the downward-facing surface. Similarly to Configuration B, slat spacing was 4.59 cm. In order to simulate manual blind operation, the following control algorithm was used (Hoffmann et al. 2016):

(1) Blinds start the day in their retracted position. As soon as Daylight Glare Index (DGI) (Chauvel et al. 1982) exceeded the threshold for discomfort (24 or "just uncomfortable") or Daylight Glare Probability (DGP) was (Wienold and Christoffersen 2006) above 0.38 (threshold for "best" classification based on the average of the 5% highest DGP values observed over a period of time (Wienold 2009)) from any of the viewpoints shown in Figure 7, the blinds are lowered for the remainder of the day[6]. This effectively assumes that occupants retract the blinds every morning when they arrive at the space.

(2) When blinds are lowered, slats are set to an angle such that there will be no downward transmission of direct solar radiation for the remainder of the day. This assumes that, from experience, occupants have a sense of how closed the slats need to be to prevent downward direct solar transmission for the time of the year.

The slat angles for the second step were determined prior to the annual simulation runs, based on preliminary glare simulations with no shading devices, in which DGI and DGP were calculated, using the Radiance *evalglare* tool, for every hour of the year, and for the viewpoints shown in Figure 7. A slat angle schedule was thus determined for every hour of the year according to the manual control algorithm detailed above. In subsequent simulations with Configuration C, this slat angle schedule was read by the shell scripts controlling the annual simulation in order to generate a Radiance model of the blind with the correct slat angle for each hour of the year.

2.2.5 Configuration Cdiff: Same as C but with mirrored slats

This configuration was modeled similarly to Configuration C in terms of operation, except that the upward-facing surface of the slats was mirrored, with 0.99 reflectance. Similarly to Configuration Bdiff, the intent of modeling this configuration was to enable the separation of the effects of slat finish and control algorithm.

2.3 Simulation cases

Annual hourly simulations were performed for a variety of

[4] Direct normal and diffuse horizontal irradiance were read from EnergyPlus weather files for the appropriate locations.

[5] Note that this criterion for when to lower the blind system is more conservative than what has generally been used for the appropriateness of using an overcast sky model for the purposes of computer simulation (see for example, IES (1984)); it leads to the blinds staying lowered for longer periods. This was done in order to reduce the possibility of glare from the sky when viewed through the unshaded glazing.

[6] The rationale for using both DGI and DGP is here aimed at more comprehensively detecting glare situations. There is evidence that in some situations DGI underestimates glare (Jakubiec and Reinhart 2012), whereas DGP can underestimate glare as well (Van Den Wymelenberg and Inanici 2014), not necessarily in the same situations.

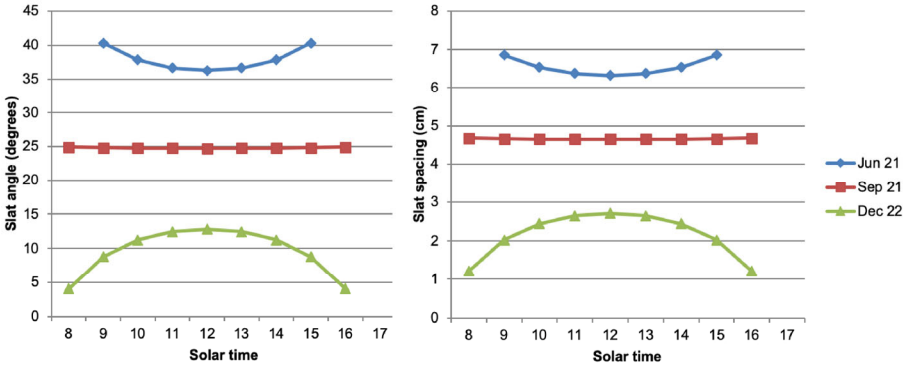

Fig. 6 Variable-spacing slat configuration: slat angle and slat spacing for south orientation and 38°N latitude, on the solstices and fall equinox

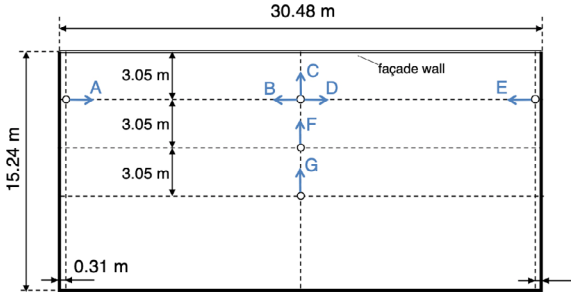

Fig. 7 Floor plan view showing position of the seven glare calculation viewpoints (A to G) inside the space

Table 3 Summary of simulation parameters

Simulation parameters	
Locations	Bakersfield (35°22′N) Oakland (37°48′N) Sacramento (38°33′N) San Diego (32°43′N)
Orientations	South, SE, East, SW, West
Window configurations	A, B, Bdiff, C, Cmirr
Calculated quantities	Horizontal illuminance Daylight glare probability

locations, orientations, window configurations, and calculated quantities. Table 3 shows the values used for those parameters.

2.3.1 Workplane illuminance

For all five upper window configurations, hourly simulations were performed for a full year at four California locations: Bakersfield, Oakland, Sacramento, and San Diego. These four locations were chosen to represent the range of climates in the most populated areas of California; they are expected to be applicable to other mid-latitude, moderately sunny areas throughout the world. Sacramento has an inland Mediterranean climate with mild winters and moderately hot and dry summers. Bakersfield has a hot desert climate. Oakland and San Diego are coastal areas with mild Mediterranean climates that include significant cloudy periods during late spring/early summer. Figure 8 shows sunshine availability data for the four climates[7] (NOAA 2020). Between April and October, the two coastal locations have significantly lower sunshine availability than the inland locations. Oakland is significantly sunnier in the spring than San Diego; San Diego is significantly sunnier than San Diego from November to February. The two inland locations have very similar sunshine availability. For the sake of brevity, this paper will present results for Oakland; results for other locations were similar and are presented in the Appendix, which is available in the Electronic Supplementary Material (ESM) in the online version of this paper. For each hourly timestep, TMY solar radiation data was used to generate a Radiance sky model using *gendaylit*, which uses the Perez sky model (Perez et al. 1990). Horizontal illuminance was calculated throughout the space at points lying on a 61 cm × 61 cm (24 inch × 24 inch) grid, at a workplane height of 76 cm (29.9 inches). This grid covered the areas of the space that were between 4.6 m and 12.2 m from the window. It is assumed that areas closer to the window would normally be reasonably well lit by the view part of the window and therefore not of interest in assessing the potential performance of the proposed light-redirecting system. The simulation was run on a Linux cluster using up to 288 CPU cores with clock speeds of between 2.3 and 2.66 GHz. The photon maps were generated with 2 million photons for global photon maps and 5 million for caustic photon maps. *Rtrace* was used with the -I option (calculate illuminance at point) and a photon map bandwidth of 200; non-default parameters were -ad 4096 -as 1024 -dp 8192 -ss 1024 -st 0 -lw 5e-6[8]. These parameters were selected to achieve as much accuracy as possible while keeping computation time under 24 hours for an annual simulation with hourly time steps. When compared with results from a full (i.e., not using forward ray-tracing methods like

[7] In two cases, Bakersfield and Oakland, sunshine availability data is not available for that city. Here we show data for the nearest available location with a comparable climate: Fresno and San Francisco, respectively.

[8] The parameter abbreviations shown here correspond to Radiance rendering parameters *ambient divisions*, *ambient super-samples*, *direct pretest density*, *specular sampling*, *specular threshold*, and *limit weight*, respectively. A good introduction to the meaning of Radiance parameters can be found in Ward Larson and Shakespeare (1998).

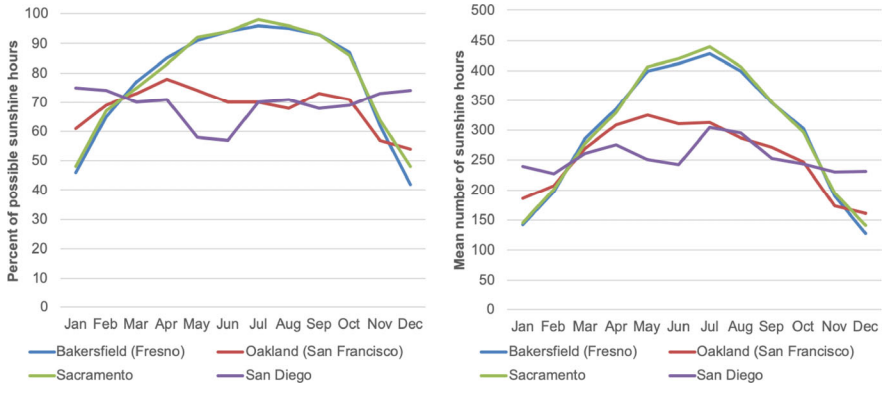

Fig. 8 Percent of possible sunshine hours and average monthly sunshine hours for Bakersfield, Oakland, Sacramento and San Diego (for Bakersfield and Oakland, data for Fresno and San Francisco is shown, respectively)

mkillum or photon mapping), five-ambient-bounce Radiance ray-tracing with the same parameters, results showed negligible differences, but the computation time was significantly shorter when using photon mapping.

2.3.2 *Glare*

In order to assess glare performance, hourly computer simulations were conducted for the whole year at seven representative viewpoints inside the space (Figure 7). Radiance parameters were selected to achieve as much accuracy as possible while keeping computation acceptable for an annual simulation with hourly time steps. Photon maps were generated with the same parameters as in the section above for workplane illuminance. Non-default Radiance parameters used for the *rpict* program were: -x 800 -y 800 -dp 1024 -ss 64 -t 60 -pj 0.2[9]. Bandwidth was 200 for global photons and variable between 1 and 5000 for caustic photons. Viewpoints were situated 120 cm (47.2 inches) above the floor (seated height). Figure 9 shows the field of view from each of the viewpoints. For each viewpoint, daylight glare probability (DGP) was determined using the Radiance *evalglare* tool. For each orientation (South, SW, West, SE, East), DGP for each one of the four window configurations were classified according to Table 4 (Wienold 2009).

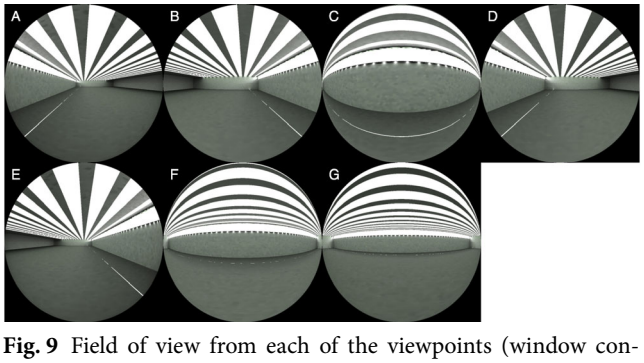

Fig. 9 Field of view from each of the viewpoints (window configuration shown is the proposed system on an equinox at local apparent solar noon). Each luminous stripe on the ceiling results from light redirection by a single slat. These luminous stripes occur up to 12 m from the window; this results from slat angle being set so that light redirection depth is 12 m

[9] The parameter abbreviations shown here correspond to Radiance rendering parameters *maximum x resolution*, *maximum y resolution*, *direct pretest density*, *specular sampling*, *time between progress reports*, and *pixel sample jitter*, respectively.

Table 4 DGP classification

95th percentile DGP	Average of top 5% DGPs	Class	Interpretation
≤ 0.35	≤ 0.38	A	Best
	> 0.38	B	Good
≤ 0.40	≤ 0.42	B	Good
	> 0.42	C	Reasonable
≤ 0.45	≤ 0.53	C	Reasonable
	> 0.53	D	Discomfort
> 0.45		D	Discomfort

3 Results

The daylighting characteristics of the proposed system can be observed from renderings of the ceiling for each configuration. For example, Figure 10 shows the ceiling of the room (the façade is at the bottom, the back of the space at the top) near the spring equinox (March 14), with the proposed system (Configuration A) and a reflective blind with conventional spacing set at the same slat angle. Although both systems are able to redirect light to 12 m (39.4 ft), the proposed system is able to consistently redirect more solar flux onto the ceiling than the conventional mirrored blind. Figure 11 shows the appearance of the space, seen from position A (see Figures 7 and 9) throughout the fall equinox (September 21) for south orientation in Oakland. Figure 12(a) shows the luminance distribution in the space at noon (local apparent solar time), for south orientation in Oakland. Figures 12(b)–12(d) show slat angle throughout the year for all five configurations, for the same orientation and location.

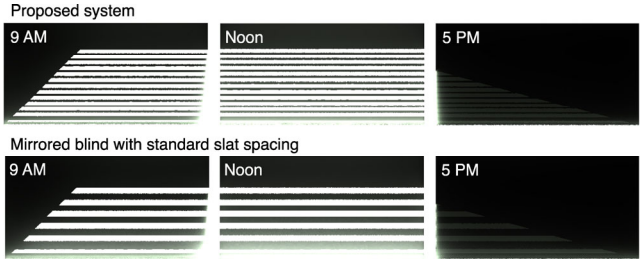

Fig. 10 Rendering of ceiling for clear sky conditions on March 14 for proposed system and a mirrored blind with standard slat spacing. Facade is south-facing. Time shown is local apparent solar time. Latitude is 38°N, close to the latitude of Oakland

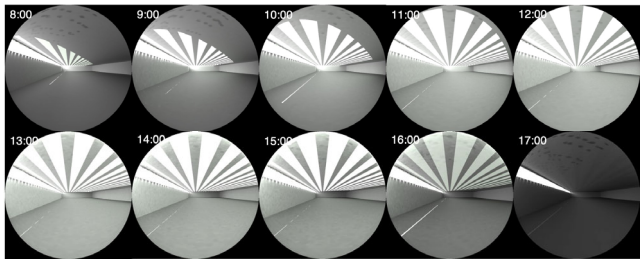

Fig. 11 Fisheye view of the space from position A (see Figs. 7 and 9) on the fall equinox (September 21), under clear sky, for south façade orientation in Oakland. Window system is Configuration A. Time shown is local apparent solar time

Figure 13 shows horizontal illuminance at workplane height (76 cm above the floor) along the centerline of the room, on an axis perpendicular to the façade, also for March 18, at solar noon. The proposed system provides higher workplane illuminance than a mirrored blind with conventional spacing set at the same slat angle. Both specularly-reflective systems deliver light more effectively to the 4.6-12.2 m zone – usually beyond the reach of daylighting systems – than diffuse white blinds or an opening without blinds, but the proposed system is markedly more effective than mirrored blinds with conventional spacing.

3.1 Daylight availability

To quantify the amount of daylight provided throughout the year, the spatial daylight autonomy (sDA) metric (IES 2012) was used. In this metric, $sDA_{X,Y}$ represents the fraction of the floor area (represented as a value between 0 and 1, or 0 and 100%) that meets a certain horizontal daylight illuminance threshold (X, usually 300 lx) for at least a certain percentage of the year (Y, usually 50%). Figure 14 shows, for Oakland climate and five façade orientations (south, southwest, west, southeast, and east), the values of $sDA_{300,10}$, $sDA_{300,20}$, $sDA_{300,30}$, $sDA_{300,40}$, $sDA_{300,50}$, $sDA_{300,60}$, $sDA_{300,70}$ and $sDA_{300,80}$ for the five configurations. Results for the other three locations did not differ significantly and are shown in the Appendix, which is available in the Electronic Supplementary Material (ESM) in the online version of this paper. The sDA calculations were performed for the 4.6–12.2 m deep zone of the space.

The proposed system (Configuration A) provides a significant amount of the lighting needs of the space through daylight alone, especially for south, southwest and southeast orientations, and significantly more so than the other four configurations. The manually-operated diffuse blinds (Configuration C) do not provide significant amounts of

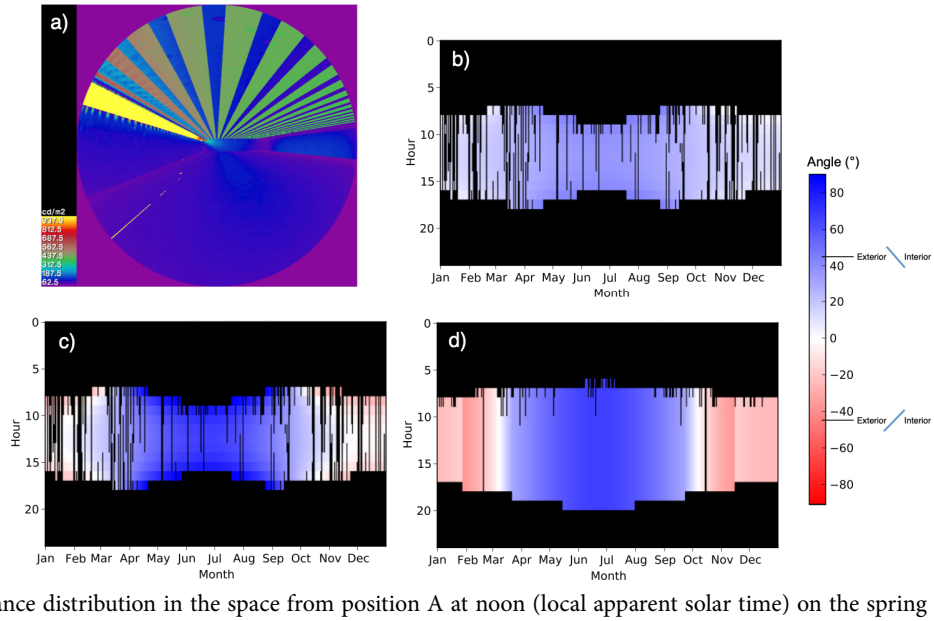

Fig. 12 (a) Luminance distribution in the space from position A at noon (local apparent solar time) on the spring equinox (March 21) for south façade orientation in Oakland. Window system is Configuration A. (b) Configuration A slat angle for south façade orientation in Oakland. (c) Configuration B/Bdiff slat angle for south façade orientation in Oakland. (d) Configuration C/Cmirr slat angle for south façade orientation in Oakland

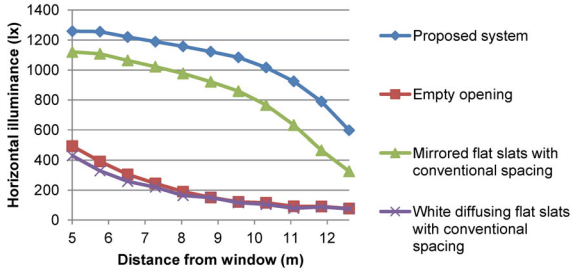

Fig. 13 Workplane illuminance along center axis of the room in the 4.6–12.2 m deep zone at solar noon on March 18 under a clear sky, for south orientation and latitude of 38°N (Oakland)

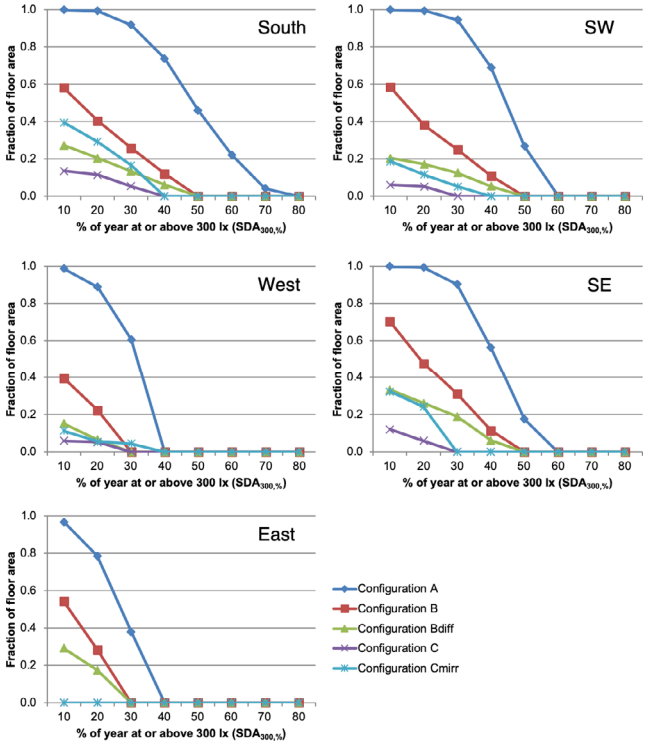

Fig. 14 Spatial daylight autonomy for five façade orientations in Oakland

daylight to the 4.6–12.2 m deep zone. The conventional automated reflective blind (Configuration B) has performance roughly in the middle between Configurations A and C. Configurations Bdiff and Cmirr perform at varying levels between Configurations B and C. For all configurations, performance across the four locations is similar.

3.2 Lighting energy[10]

The potential lighting energy savings from each configuration were determined by calculating the amount of electrical energy needed to provide a useful level of illumination throughout the space. This was done by assuming an installed power density of 8.07 W/m^2 [11], a design workplane illuminance of 300 lx, power consumption that is directly proportional to light output (i.e., 50% power would provide 150 lx, a not unreasonable approximation for LED light sources [12]), and 10 hours of building operation per day (8 AM to 6 PM standard time), 365 days per year. For each point in the 61 cm × 61 cm grid used in the workplane illuminance simulations, and for each hour from 8 AM to 6 PM, for every day of the year, the fraction of full electrical power ϕ was calculated by:

$$\begin{cases} \phi = \dfrac{E}{300\ \text{lx}} & \text{if } E \le 300\ \text{lx} \\ \phi = 1 & \text{if } E > 300\ \text{lx} \end{cases} \tag{5}$$

where E is the horizontal illuminance. That fraction was then averaged over time and space in the same step in order to obtain an annually averaged power fraction:

$$\phi_{\text{avg}} = \frac{\sum_{\substack{1 \le d_{\text{year}} \le 365 \\ 9 \le h_{\text{day}} \le 18}} E\left(d_{\text{year}}, h_{\text{day}}\right)}{365 \times 10} \tag{6}$$

where ϕ_{avg} is the average power fraction, d_{year} the day of the year, h_{day} the hour of the day, and $E(d_{\text{year}}, h_{\text{day}})$ the horizontal illuminance on day d_{year} and hour h_{day} [13]. Average annual lighting power consumption is shown for Oakland in Table 5. The annual energy consumption density per floor area shown in the table was calculated assuming 5 days of operation per week and 50 weeks of operation per year; the table also shows percentage lighting energy savings when compared to Configuration C.

3.3 Glare

Table 6 shows annual DGP classification (see Table 4 for reference) for each of the views for the Sacramento climate. While there were some variations between climates, results did not differ significantly in terms of how the different evaluated configurations compared to each other. Hours used in analysis were 8 AM to 6 PM local time. Results show that, in terms of visual comfort, the proposed system generally provides acceptable to excellent visual comfort (depending on climate and orientation). Configuration B has worse performance, often leading to situations of clear

[10] The lighting energy savings estimates developed in this section are intended as a general indication of the potential of the proposed light redirecting slat system for reducing the need for electric lighting. The illuminance target used, 300 lx, is a commonly used design target for office spaces. Performance for specific electric lighting systems will vary according to factors including light source type and luminaire efficacy.

[11] This corresponds to 0.75 W/ft^2, the maximum installed lighting power density in general office spaces allowed by the 2016 California building code for office areas greater than 23.2 m^2 (250 ft^2) (CEC 2016).

[12] This also assumes that standby power is zero.

[13] Note that h_{day} takes the value n for the nth hour of the day. For example, the value of h_{day} is 9 for the timestep that comprises the time between 8 AM and 9 AM.

Table 5 Average power level, average lighting power density, annual lighting energy consumption and percentage savings for Oakland climate

		Orientation				
	Configuration	South	SW	West	SE	East
Average power level (% of full power)	A	34%	44%	64%	48%	64%
	B	58%	62%	76%	62%	75%
	Bdiff	65%	71%	82%	69%	79%
	C	72%	73%	71%	76%	98%
	Cmirr	62%	64%	64%	66%	98%
Average LPD (W/m^2)	A	2.77	3.59	5.17	3.88	5.16
	B	4.65	5.01	6.14	4.98	6.02
	Bdiff	5.24	5.75	6.62	5.53	6.37
	C	5.83	5.87	5.71	6.10	7.92
	Cmirr	5.04	5.18	5.19	5.29	7.87
Annual consumption ($kWh/(m^2 \cdot a)$)	A	6.9	9.0	12.9	9.7	12.9
	B	11.6	12.5	15.4	12.4	15.0
	Bdiff	13.1	14.4	16.6	13.8	15.9
	C	14.6	14.7	14.3	15.2	19.8
	Cmirr	12.6	13.0	13.0	13.2	19.7
% savings vs. Configuration C	A	52%	39%	9%	36%	35%
	B	20%	15%	−8%	18%	24%
	Bdiff	10%	2%	−16%	9%	20%
	Cmirr	14%	12%	9%	13%	1%

Table 6 DGP class for viewpoints A to G in Oakland

		Orientation				
Viewpoint	Configuration	South	SW	West	SE	East
A	A	A	A	A	A	A
	B	C	A	A	Discomfort	Discomfort
	Bdiff	A	A	A	A	A
	C	A	A	A	A	A
	Cmirr	Discomfort	A	A	A	A
B	A	A	A	A	A	A
	B	Discomfort	Discomfort	C	B	A
	Bdiff	A	A	A	A	A
	C	A	A	A	A	A
	Cmirr	Discomfort	A	A	A	A
C	A	B	B	A	C	C
	B	Discomfort	Discomfort	Discomfort	Discomfort	Discomfort
	Bdiff	C	C	A	C	C
	C	A	A	A	A	A
	Cmirr	Discomfort	B	B	C	A
D	A	A	A	A	A	A
	B	C	A	A	Discomfort	Discomfort
	Bdiff	A	A	A	A	A
	C	A	A	A	A	A
	Cmirr	Discomfort	A	A	A	A

Table 6 DGP class for viewpoints A to G in Oakland (Continued)

Viewpoint	Configuration	Orientation				
		South	SW	West	SE	East
E	A	A	A	A	A	A
	B	Discomfort	Discomfort	C	B	A
	Bdiff	A	A	A	A	A
	C	A	A	A	A	A
	Cmirr	Discomfort	A	A	A	A
F	A	A	A	A	B	B
	B	Discomfort	Discomfort	C	Discomfort	Discomfort
	Bdiff	A	A	A	B	C
	C	A	A	A	A	A
	Cmirr	Discomfort	B	B	C	A
G	A	A	A	A	A	A
	B	C	Discomfort	B	Discomfort	B
	Bdiff	A	A	A	A	A
	C	A	A	A	A	A
	Cmirr	C	B	B	B	A

discomfort. Configuration C has the best performance of the five configurations.

4 Discussion

4.1 Lighting performance

Results show that the proposed system (Configuration A) results in significant energy savings, both when compared with a commercially available automated reflective blind (2.1–4.9 kWh/(m²·a), or 14%–42%, depending on climate and orientation; the greatest savings were obtained for a south-facing façade in Bakersfield, the smallest for an east-facing façade in Oakland) or to a manually operated venetian blind (1.4–7.9 kWh/(m²·a), or 9%–54%, depending on climate and orientation; the greatest savings were obtained for a south-facing façade in Bakersfield, the smallest for a west-facing façade in Oakland), while maintaining acceptable visual comfort.

4.2 Glare performance

In terms of glare, the proposed system shows acceptable glare performance, achieving, for Oakland climate, DGP class A performance ("best") for 29 viewpoints and orientations studied, and class C ("reasonable") performance or better for all viewpoints and orientations studied (Table 7). In comparison, Configuration B has poorer performance, with class D ("discomfort") performance for 19 viewpoint/orientation combinations. This is not entirely surprising, since, while the control algorithm for Configuration B was set so that straight-through transmission of direct solar radiation was blocked, transmission of direct solar radiation reflected by the slats was not blocked, in order to provide a "best case" scenario for daylight delivery at the expense of glare. At low sun angles, this direct solar radiation reflected by the slats can have a downward direction, reaching the occupants' eyes and causing glare. Configuration C shows the best glare performance for Oakland climate, with class A performance for 35 viewpoints/orientations. Again, this is to be expected, as the control algorithm used to simulate manual control was based on achieving specific glare metrics that all but ensured visual comfort was achieved, at the expense of the significant reduction in daylight availability relative to Configuration A that can be seen in Figure 14. It should be noted that, since electric lights were not included in the ray-tracing model, these calculations could somewhat overestimate glare levels, as electric lighting would reduce luminance ratios in the field of view, especially at viewing positions away from the window.

Table 7 Number of viewpoint/orientations per DGP class and window configuration for Oakland

Configuration	DGP Class			
	A	B	C	Discomfort
A	29	4	2	0
B	6	4	6	19
Bdiff	29	1	5	0
C	35	0	0	0
Cmirr	19	7	3	6

4.3 Feasibility considerations

The scope of the study presented in this paper was to evaluate, using computer simulation, the potential performance of a light-redirecting blind with variable slat width. Although, strictly speaking, they are outside the scope of this study, some considerations regarding the anticipated feasibility of implementing this concept in practice are discussed in this section.

Although the point of departure for the concepts explored in this paper – the venetian blind – is a mature technology, with many varieties currently in production, implementing a variable-spacing version is challenging, beyond the issue already mentioned in Section 2 of this paper regarding storage of the slats that are not needed at any point in time: adjusting slat spacing also requires each slat to move vertically a different distance from the adjacent slats. The technical problems posed by a variable slat width configuration appear easier to surmount; a prototype is under development.

Simulations indicate that the performance of the proposed system has some sensitivity to slat angle (Figure 15); although not technically infeasible, this requires a degree of attention in any physical implementation. Further research is needed to determine the impact of deviations from the design slat angle on energy savings and visual comfort.

In this study, slats with a flat, specular surface were assumed, but appropriate slat surface finish and curvature may deviate from this in practical applications. While in theory flat, specular slats offer predictable behavior, in practice a degree of diffuse reflectance may be desirable if it is necessary to soften the contrast between ceiling areas directly illuminated by the slats and adjacent areas. It may also be desirable to introduce curvature or other deviations from a simple flat surface in order to increase slat stiffness.

There are additional aspects that need to be considered in the development of a commercially-available fenestration system based on the concept presented in this paper include.

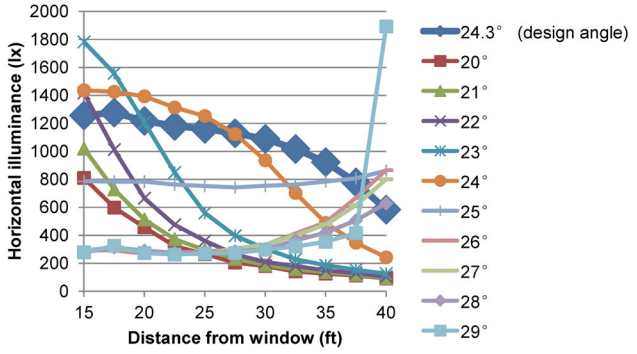

Fig. 15 Horizontal illuminance obtained with the proposed system (Configuration A) at integer slat angles within 5° of the design slat angle for 38°N latitude, south orientation and noon solar time on March 21

A successful system would need to have low maintenance requirements; it would ideally have the ability to be placed within an insulated glazing unit (IGU) with a nominal life on the order of twenty years, or between glazing with a removable access panel. It would also be self-powered, using batteries and/or photovoltaic power. Additionally, it would allow for adjustments to operation after initial commissioning, in order for operation to be reset to meet new space or user requirements. Finally, wireless communications to building management system (BMS) or equivalent would also be desirable in order for the fenestration system to operate in coordination with other building systems whenever appropriate.

4.4 Considerations regarding heating and cooling energy demand

Daylighting can save significant amounts of energy when it replaces the use of electric energy, but its impacts on heating and cooling energy demands must be considered (Mardaljevic et al. 2009). Several factors affect these impacts, including climate, building construction, the ratio between the glazed and opaque portions of the building façade, nearby obstructions, the geometry and surface properties of the interior space, and the thermal and solar optical properties of the fenestration. In general, the evidence in the literature indicates that it is possible to harness the energy benefits of daylight for a broad range of locations, building configurations and fenestration types (Lam and Li 1999; Bodart and De Herde 2002; Dubois and Blomsterberg 2011; Ochoa et al. 2012; Huang et al. 2014; Favino et al. 2015; Pellegrino et al. 2017). Heating and cooling impacts of the proposed light redirection system were outside of the scope of this study. Nevertheless, several factors suggest that these impacts would not be significant when compared with the lighting energy impacts, which were the focus of this study. In terms of HVAC impacts, two differences between the proposed light redirection system and a conventional shading system are apparent. First, the proposed system might introduce slightly more solar heat gains into the space than a conventional shading system, which reflects some amount of solar radiation back to the exterior. Second, due to the light redirection deep into the space, the solar heat gains admitted into the space might be distributed further into the space than those from a conventional shading system. However, it is important to have in mind that, while admitting enough daylight to provide useful light deep into the space, the amount of heat gain through a 61 cm high section of the façade represents a rather small part of the total cooling load of such a large space. This heat gain is also offset if the internal heat gains from electric lighting are reduced because of the increased daylight availability. Because

of the high efficacy of daylight, from an energy standpoint it is generally beneficial to use daylight instead of electric lighting, especially if the invisible components of daylight can be filtered (Lapsa et al. 2007). In the case of the system presented in this paper, this could be achieved via spectrally selective low-emissivity glazing. The benefits would partly be negated if the space is overlit using daylight; the system presented here reduces such risk by distributing the admitted daylight throughout a large area of the building interior, where it is more likely to be useful, rather than concentrating it nearer the building façade, where it would be more likely to overlight the space, with the concomitant issues of glare and overheating. It would also be possible to use electrochromic windows in combination with this system to further modulate the amount of daylight admitted into the space.

5 Conclusions

The annual lighting and visual comfort performance of a high-efficiency light redirection system based on variable-spacing reflective slats was evaluated using forward ray-tracing simulation techniques and high performance computing resources. The variable slat spacing allows consistent light redirection into the deep (4.6–12.2 m) zone of open-plan floorplans without allowing any straight-through downward transmission of direct solar radiation. This effectively allows this light-redirecting system to redirect all incident direct solar radiation in an upward direction, allowing none to reach occupants' eyes. Computer simulations for four mid-latitude climates showed significant energy savings when compared with conventional automated reflective blinds (2.1–4.9 kWh/(m^2·a), or 14%–42%, depending on climate and orientation; the greatest savings were obtained for a south-facing façade in Bakersfield, the smallest for an east-facing façade in Oakland) or, especially, manually-operated matte white venetian blinds (1.4–7.9 kWh/(m^2·a), or 9%–54%, depending on climate and orientation; the greatest savings were obtained for a south-facing façade in Bakersfield, the smallest for a west-facing façade in Oakland), while maintaining acceptable to excellent visual comfort conditions throughout the interior space. Several issues relevant for the practical implementation of this concept have been explored and discussed in this paper. The variable slat width configuration of the high-efficiency redirection system proposed here appears to be more feasible to implement than the variable slat spacing configuration; a prototype is in development. Calculations show that the performance of this type of system will be affected by the accuracy with which the slat angle can be set. While the admission of light through the façade can have a negative impact on cooling loads, this system does not appear to be significantly different from conventional shading in that respect, merely distributing further into the space the radiation that normally would be absorbed somewhere nearer the façade. The introduction of excessive light into the space could easily be mitigated by operating the system in a less efficient manner, for example by setting the reflective slats at a suboptimal angle, or using an auxiliary method, such as electrochromic windows, for modulating the amount of radiation introduced through the façade.

Acknowledgements

The authors would like to acknowledge Gregory Ward (Anyhere Software), Taoning Wang (LBNL) for discussions regarding Radiance modeling; Mudit Saxena (Vistar Energy), Lisa Heschong, and Hayden McKay (Horton Lees Brogden Lighting Design) for suggestions on the modeling approach; and Daniel Fuller (LBNL) for critical support with computing infrastructure. This work was supported by the California Energy Commission through its Electric Program Investment Charge (EPIC) Program on behalf of the citizens of California and by the Assistant Secretary for Energy Efficiency and Renewable Energy of the U.S. Department of Energy under Contract No. DE-AC02-05CH11231.

Electronic Supplementary Material (ESM): supplementary material is available in the online version of this article at https://doi.org/10.1007/s12273-020-0674-6.

References

3M (2017). Enhanced Specular Reflector (3M ESR). Available at https://www.3m.com/3M/en_US/company-us/all-3m-products/~/3M-Enhanced-Specular-Reflector-3M-ESR?N=5002385+3293061534&rt=rud. Accessed 18 Mar 2019.

Aiziewood ME (1993). Innovative daylighting systems: an experimental evaluation. *Lighting Research and Technology*, 25: 141–152.

Alva M, Vlachokostas A, Madamopoulos N (2020). Experimental demonstration and performance evaluation of a complex fenestration system for daylighting and thermal harvesting. *Solar Energy*, 197: 385–395.

Andersen M, Rubin M, Scartezzini J-L (2003). Comparison between ray-tracing simulations and bi-directional transmission measurements on prismatic glazing. *Solar Energy*, 74: 157–173.

Athienitis AK, Tzempelikos A (2002). A methodology for simulation of daylight room illuminance distribution and light dimming for a room with a controlled shading device. *Solar Energy*, 72: 271–281.

Baker NV, Fanchiotti A, Steemers K (1993). Daylighting in architecture: An European Reference Book. London: James & James.

Beltran LO, Lee ES, Selkowitz SE (1996). Advanced optical daylighting systems: Light shelves and light pipes. In Proceedings of the IESNA Annual Conference, Cleveland, OH, USA.

Cossmann J (1905). US Patent Office, Patent No. 792,759.

Bodart M, de Herde A (2002). Global energy savings in offices buildings by the use of daylighting. *Energy and Buildings*, 34: 421–429.

CEC (2016). Building energy efficiency standards for residential and nonresidential buildings. California Energy Commission, CEC-400-2015-037-CMF.

Chauvel P, Collins JB, Dogniaux R, Longmore J (1982). Glare from windows: current views of the problem. *Lighting Research and Technology*, 14: 31–46.

Dubois M-C, Blomsterberg Å (2011). Energy saving potential and strategies for electric lighting in future North European, low energy office buildings: A literature review. *Energy and Buildings*, 43: 2572–2582.

Eacret KM (1977). Beamed daylighting—Historical survey, current prototype testing, and design options. Master Thesis, University of California, USA.

Ewen JM (1897). US Patent Office, Patent No. 595,263.

Favoino F, Overend M, Jin Q (2015). The optimal thermo-optical properties and energy saving potential of adaptive glazing technologies. *Applied Energy*, 156: 1–15.

Hashemi A (2014). Daylighting and solar shading performances of an innovative automated reflective louvre system. *Energy and Buildings*, 82: 607–620.

Heim D, Kieszkowski K (2006). Shading devices designed to achieve the desired quality of internal daylight environment. In: Proceedings of the 23rd Conference on Passive and Low Energy Architecture (PLEA 2006), Geneva, Switzerland.

Hoffmann S, Lee ES, McNeil A, Fernandes L, Vidanovic D, Thanachareonkit A (2016). Balancing daylight, glare, and energy-efficiency goals: An evaluation of exterior coplanar shading systems using complex fenestration modeling tools. *Energy and Buildings*, 112: 279–298.

Huang Y, Niu J, Chung TM (2014). Comprehensive analysis on thermal and daylighting performance of glazing and shading designs on office building envelope in cooling-dominant climates. *Applied Energy*, 134: 215–228.

IES (1984). Recommended practice for the calculation of daylight availability. *Journal of the Illuminating Engineering Society*, 13: 381–392.

IES (2000). The IESNA Lighting Handbook, 9th edn. New York: Illuminating Engineering Society of North America.

IES (2012). Approved method: IES Spatial Daylight Autonomy (sDA) and Annual Sunlight Exposure (ASE), IES LM-83-12. New York: Illuminating Engineering Society of North America.

Jakubiec JA, Reinhart CF (2012). The 'adaptive zone'—A concept for assessing discomfort glare throughout daylit spaces. *Lighting Research and Technology*, 44: 149–170.

Konis K, Lee ES (2015). Measured daylighting potential of a static optical louver system under real sun and sky conditions. *Building and Environment*, 92: 347–359.

Kristensen PE (1994). Daylighting technologies in non-domestic buildings. *International Journal of Solar Energy*, 15: 55–67.

Laar M, Grimme FW (2002). German developments in guidance systems: An overview daylight. *Building Research & Information*, 30: 282–301.

Lam JC, Li DHW (1999). An analysis of daylighting and solar heat for cooling-dominated office buildings. *Solar Energy*, 65: 251–262.

Lapsa MV, Maxey LC, Earl DD, Beshears DL, Ward CD, Parks JE (2007). Hybrid solar lighting provides energy savings and reduces waste heat. *Energy Engineering*, 104: 7–20.

Lee ES, DiBartolomeo DL, Selkowitz SE (1998). Thermal and daylighting performance of an automated Venetian blind and lighting system in a full-scale private office. *Energy and Buildings*, 29: 47–63.

Lee ES, Geisler-Moroder D, Ward G (2018). Modeling the direct sun component in buildings using matrix algebraic approaches: Methods and validation. *Solar Energy*, 160: 380–395.

Li Y, Köster H, Bruegge B (2015). Software to determine the energy and light transmission of glass facades in conjunction with special daylight redirecting systems. In: Proceedings of the 14th International Conference on Sustainable Energy Technologies, Nottingham, UK.

Littlefair PJ (1990). Innovative daylighting: Review of systems and evaluation methods. *Lighting Research and Technology*, 22: 1–17.

Littlefair PJ (1995). Light shelves: Computer assessment of daylighting performance. *Lighting Research and Technology*, 27: 79–91.

Mardaljevic J, Heschong L, Lee E (2009). Daylight metrics and energy savings. *Lighting Research and Technology*, 41: 261–283.

McGuire ME (2005). A system for optimizing interior daylight distribution using reflective venetian blinds with independent blind angle control. Master Thesis, Massachusetts Institute of Technology, Cambridge, USA.

McNeil A, Lee ES, Jonsson JC (2017). Daylight performance of a microstructured prismatic window film in deep open plan offices. *Building and Environment*, 113: 280–297.

Moro JL (2019). Glasprodukte. In: Baukonstruktion – vom Prinzip zum Detail. Berlin: Springer.

NOAA (2020). 1961–1990 Global Climate Normals. National Oceanic and Atmospheric Administration, Available at ftp://ftp.atdd.noaa.gov/pub/GCOS/WMO-Normals/TABLES/. Access 4 Mar 2020.

Ochoa CE, Aries MBC, van Loenen EJ, Hensen JLM (2012). Considerations on design optimization criteria for windows providing low energy consumption and high visual comfort. *Applied Energy*, 95: 238–245.

Pellegrino A, Cammarano S, Lo Verso VRM, Corrado V (2017). Impact of daylighting on total energy use in offices of varying architectural features in Italy: Results from a parametric study. *Building and Environment*, 113: 151–162.

Pennycuick JM (1885). US Patent Office, Patent No. 312,290

Perez R, Ineichen P, Seals R, Michalsky J, Stewart R (1990). Modeling daylight availability and irradiance components from direct and global irradiance. *Solar Energy*, 44: 271–289.

Rosenfeld AH, Selkowitz SE (1977). Beam daylighting: An alternative illumination technique. *Energy and Buildings*, 1: 43–50.

Ruck NC (1985). Beaming daylight into deep rooms. *Batiment International, Building Research and Practice*, 13: 144–147.

Ruck N, Aschehoug Ø, Aydinli S, Christoffersen J, Courret G, et al. (2001). Daylight in Buildings. A Source Book on Daylighting Systems and Components. Available at https://facades.lbl.gov/sites/all/files/daylight-in-buildings.pdf

Schregle R (2015). The Radiance photon map extension user manual, Revision 1.10. Available at https://www.radiance-online.org/learning/documentation/photonmap-user-guide.

Sweitzer G (1993). Three advanced daylighting technologies for offices. *Energy*, 18: 107–114.

Thanachareonkit A, Lee ES, McNeil A (2014). Empirical assessment of a prismatic daylight-redirecting window film in a full-scale office testbed. *Leukos*, 10: 19–45.

Thuot K, Andersen M (2011). A novel louver system for increasing daylight usage in buildings. In: Proceedings of the 27th Conference on Passive and Low Energy Architecture (PLEA 2011), Louvain-la-Neuve, Belgium.

Tregenza PR (1995). Mean daylight illuminance in rooms facing sunlit streets. *Building and Environment*, 30: 83–89.

Tsangrassoulis A (2008). A review of innovative daylighting systems. *Advances in Building Energy Research*, 2: 33–56.

Tsangrassoulis A (2016). Shading and daylight systems. In: Boemi SN, Irulegi O, Santamouris M (eds), Energy Performance of Buildings. Cham, Switzerland: Springer International Publishing, pp. 437–466.

Van Den Wymelenberg K, Inanici M (2014). A critical investigation of common lighting design metrics for predicting human visual comfort in offices with daylight. *Leukos*, 10: 145–164.

Wong IL (2017). A review of daylighting design and implementation in buildings. *Renewable and Sustainable Energy Reviews*, 74: 959–968.

Ward Larson G, Shakespeare R (1998). Rendering with Radiance: The Art and Science of Lighting Visualization. San Francisco: Morgan Kaufman.

Wienold J, Christoffersen J (2006). Evaluation methods and development of a new glare prediction model for daylight environments with the use of CCD cameras. *Energy and Buildings*, 38: 743–757.

Wienold J (2009). Dynamic daylight glare evaluation. In: Proceedings of the 11th International IBPSA Building Simulation Conference, Glasgow, UK.

Yip S, Chen Y, Athienitis A (2015). Comparative analysis of a passive and active daylight redirecting blind in support of early stage design. In: Proceedings of CISBAT 2015, Lausanne, Switzerland.